Physiological causes and biogeographic consequences of thermal optima in the hypoxia tolerance of marine ectotherms

Martin-Georg Alexander Endress

A thesis
submitted in partial fulfillment of the
requirements for the degree of

Master of Science

University of Washington
2021

Committee:
Curtis Deutsch
Timothy Essington

Program Authorized to Offer Degree:
Quantitative Ecology and Resource Management

University of Washington

Abstract

Physiological causes and biogeographic consequences of thermal optima
in the hypoxia tolerance of marine ectotherms

Martin-Georg Alexander Endress

Chair of the Supervisory Committee:
Curtis Deutsch
School of Oceanography

Recent measurements of critical O_2 thresholds ('P_{crit}') in aquatic animals have revealed thermal optima in their hypoxia tolerance. To discern the prevalence, physiological drivers, and biogeographic manifestations of such P_{crit} curves, this research investigates experimental and occurrence data using a dynamic model of aquatic water breathers. The model simulates the transfer of O_2 from ambient water into animal tissues driven by temperature-dependent rates of metabolism, diffusion, and ventilatory and circulatory systems with O_2-protein binding. Results show that thermal optima in P_{crit} can arise even when all physiological rates increase steadily with temperature. This occurs when O_2 supply at low temperatures is limited by a process that is more temperature sensitive than metabolism, and when O_2 supply at warmer temperatures is limited by a less sensitive process. Analysis of species respiratory traits suggests this scenario is not uncommon in marine biota, with ventilation and circulation limiting supply under cold conditions and diffusion limiting supply under warm conditions. State-space habitats reveal that species with these physiological traits inhabit lowest O_2 waters near the optimal temperature for hypoxia tolerance, and are restricted to higher O_2 at temperatures above and below this optimum. These results imply that tolerance to low oxygen can decline under cold and warm conditions and may influence species range limits.

Significance Statement

Physiology shapes the ecology, biogeography, and climate responses of marine species. In aquatic ectotherms, accelerating metabolism and lowered oxygen availability generally result in increasing oxygen limitation with warming. Here we present evidence for thermal optima in hypoxia tolerance of diverse species that is explained by a dynamical model of organismal physiology. Our results indicate that this potentially widespread bidirectional pattern explains species biogeographic limits in cold and warm waters. It can be understood using a generalized Metabolic Index of O_2 supply to demand, which captures the variable observed trends between temperature and species hypoxia sensitivity. Oxygen limitation of aerobic metabolism in cold water has far-reaching implications for marine biogeography, species migrations under climate warming and habitat loss from global cooling.

Introduction

Climate change is raising temperatures throughout the upper ocean, while decreasing its oxygen content. These trends are among the most robustly observed and well understood aspects of global ocean change (e.g. 1, 2, 3, 4). They also pose a major challenge for marine ectotherms, whose metabolic rates rise exponentially with temperature (5), requiring a concomitant increase in O_2 supply to maintain aerobic energy balance. Patterns of O_2 loss and ocean heat uptake coupled with known physiological tolerances suggest that this balance is already limiting the geographic range of many species, most commonly at the equatorial (warm) and/or deep (low O_2) edge of species distributions (6, 7, 8, 9).

The environmental O_2 minimum at which an organism can sustain its resting metabolism is typically reported as a critical pressure (P_{crit}, 10) and remains the most common measure of hypoxia tolerance (e.g. 11), despite potential complexities of experimental determination (12, 13). In most studied species, P_{crit} increases with temperature, implying that their O_2 demand accelerates faster with warming than their supply (14).

In contrast, laboratory respirometry has revealed a wide range of more complex relationships between temperature and P_{crit}. Some species show a decrease in P_{crit} as temperatures rise, implying that supply accelerates faster than demand, although this has rarely been observed (but see 15, 16). In recent experiments, still other species exhibit both a decline in P_{crit} as temperatures rise from the coldest water, followed by an increase from further warming, resulting in patterns that are broadly 'bowl-shaped' with respect to temperature (17, 18). While the individual processes of supply and demand all tend to increase steadily with temperature (19, 20), these bowl-shaped P_{crit} curves require that the temperature dependence of either net O_2 supply or demand follow more complex relationships. Such thermal optima for hypoxia tolerance have long been posited (21, 22), but lack a quantitative understanding. This prevents a mechanistic evaluation of the role of hypoxia tolerance at the cold edge of range limits, and the associated implications of climate change, especially for populations not living near a species' warm and/or low-O_2 range limit, and during periods of global cooling.

To examine the prevalence of thermal optima in hypoxia tolerance, diagnose the physiological conditions under which it can arise, and evaluate its relevance to species biogeography, we combined new laboratory experiments, a dynamic model of O_2 supply in marine ectotherms, and species biogeographic distribution data. Among all studied species, we find complex P_{crit} behavior across a broad temperature range. A general model of aquatic water breathers demonstrates the conditions under which thermal optima can emerge from the multi-step nature of the O_2 supply chain, and suggests that marine species commonly meet those conditions. The behavior of the dynamic model can be reproduced with a generalized Metabolic Index (MI) of O_2 supply to demand (9) that captures a wide range of observed P_{crit} curves. Finally, we present evidence that P_{crit} curves with a thermal optimum are also reflected in the biogeography of marine species and thus may explain the cold/poleward limit in such species geographic ranges.

Results

Laboratory Observations

To evaluate the prevalence of non-exponential P_{crit} curves, we measured P_{crit} across a wide temperature spectrum for four previously unmeasured invertebrate species. These species span four different phyla, have multiple modes of oxygen supply, and regularly encounter temporal and/or spatial variability in environmental pO_2 (Fig. 1). Following published respirometry protocols (Materials and Methods), we conducted P_{crit} measurements from the freshwater oligochaete worm *Tubifex tubifex*, the outer shelf/upper slope sea urchin *Lytechinus pictus* from California, and the Atlantic intertidal anemone *Nematostella vectensis*. We also used P_{crit} measurements of the squid *Doryteuthis opalescens* which is exposed to strong gradients of temperature and O_2 in the California Current System (23).

Measurements of all species reveal a minimum in P_{crit} at intermediate experimental temperatures, with substantial variation in the location of the thermal optimum and depth of the P_{crit} minimum. Some species P_{crit} curves reveal a broad bowl (*L. pictus*), others a deep bowl (*T. tubifex*), and

still others a relatively constant P_{crit} at cold temperatures, followed by a sharp rise at warmer temperatures (*N. vectensis, D. opalescens*). These new respirometry data combined with published data (17,18), indicate that thermal optima in hypoxia tolerance are found in multiple phyla and across multiple modes of oxygen supply (e.g., gills and a blood vascular system in squid versus cutaneous respiration in anemones) and may therefore represent a widespread pattern.

Dynamic Model

To explore the conditions that lead to a thermal optimum in hypoxia tolerance, we develop a dynamic model of O_2 supply and demand in water-breathing animals. The model simulates the transfer of O_2 from the environment to the metabolizing tissues of an organism across a range of temperatures using a system of coupled non-linear ordinary differential equations (ODEs). To make the model generally applicable to aquatic animals, we include all the potential pools and fluxes of O_2, including external ventilation of water from the ambient fluid to the boundary layer at the exchange surface, the molecular O_2 diffusion across that surface, and internal flux of O_2 to metabolizing body tissues, which may be mediated by a circulatory system (Fig. 2A). In addition to dissolved O_2, the model also tracks the concentration of the bound and unbound forms of an oxygen-transport protein such as hemoglobin or hemocyanin (denoted HxO and Hx, respectively), which bind and release molecular O_2 according to the associated chemical equilibrium. This is captured by the pO_2 at half-saturation (denoted P_{50}) and the enthalpy (ΔH) of the binding reaction, which governs the temperature dependence of that equilibrium (24, details SI).

Each of the three O_2 supply processes (ventilation, diffusion, and circulation) is described by a rate S_i that is represented as the product of the pO_2 difference between the respective compartments, $\Delta_i pO_2$, and a temperature-dependent rate coefficient $\hat{\alpha}_i(T)$ that characterizes the kinetics of that process:

$$S_i(T) = \hat{\alpha}_i(T)\Delta_i pO_2 \tag{1}$$

The temperature-dependency of the three rate coefficients – flow rates of ventilated water and circulated blood, and the diffusivity of O_2 – each vary exponentially with temperature (Arrhenius function), as does the metabolic rate, but with distinct temperature sensitivities. The resulting 8 parameters (3 supply rate coefficients, the metabolic rate, and the temperature sensitivity of each) along with the 3 chemical parameters (P_{50}, ΔH and total Hx concentration) represent a set of traits that determine a model organism's hypoxia tolerance and its variation with temperature. The well-documented trait variations in real animals (e.g., overall O_2 supply capacity [25] and adaptation to hypoxia [26], gill surface area [27, 28], blood properties [29, 30]) are simulated by scaling these parameters in the model. Our analysis aims to discern how such biological traits govern the shape of the resulting P_{crit} curves with respect to temperature.

Model simulations resemble standard closed system respirometry experiments used to determine P_{crit} values (Fig. 2B, 31), in which O_2 is depleted from the ambient water as it gets transferred to metabolizing tissues. Both the O_2 concentrations and the fraction of O_2-bound protein (HxO) decline in all compartments. Once O_2 levels in the tissue compartment can no longer support resting metabolism, consumption slows down with the onset of hypoxemia, allowing P_{crit} to be diagnosed from the rate of environmental O_2 depletion using breakpoint analysis (Materials and Methods, full model in SI).

Simulations across a range of temperatures yield the P_{crit} curve, which integrates the contribution of all traits to a single metric of hypoxia tolerance. Across a wide range of model parameters centered on the most common traits observed in marine organisms (14), the P_{crit} curves exhibit an overall rise with temperature, driven by the increase in metabolic rate.

Both the chemical properties (Hx, ΔH and p50) as well as the rate coefficients of supply and demand ($\hat{\alpha}_i$) have intuitive impacts on the P_{crit} curves. For example, a higher concentration of total Hx acts to lower the P_{crit} curve across all temperatures (Fig. 2C), enhancing the tolerance to hypoxia. An equivalent effect can be obtained by increasing the biophysical supply coefficients, simulating changes such as a larger gill area or faster ventilation rate (Fig. 2D).

However, we also find less intuitive impacts on the slope and curvature of the curves. For instance, a

25 % increase in the ventilation rate does not lower the P_{crit} by the same fraction at all temperatures, but instead has a larger impact under cold conditions than under warm conditions (Fig. 2D). In other words, the P_{crit} curves resulting from a multi-step supply chain can depart from simple exponential relationships with temperature, even when each single supply process accelerates exponentially with warming.

We conclude that the well-known non-linearities in blood-O_2 binding are not the essential cause of this behavior, because the variation due to biophysical properties is similar to that induced by variations in blood chemistry. Moreover, we observe complex P_{crit} curves in organisms without O_2-binding proteins (e.g. *N. vectensis* in Fig. 1).

Instead, we focus our analysis on the mechanisms by which the linear combination of biophysical transfer processes in a multi-step O_2 supply chain leads to the complex patterns observed in P_{crit} curves. The result is demonstrated quantitatively in a model with a supply chain consisting only of ventilation and diffusive gas exchange (Fig. 3). In isolation, each step yields a simple (exponential) P_{crit} curve with a slope depending on the temperature sensitivities of supply and demand. The curve is increasing if metabolic demand accelerates faster with temperature than supply (shown for diffusion, Fig. 3A), and decreasing if instead the temperature sensitivity of supply exceeds that of metabolism (ventilation, Fig. 3B). Combining ventilation and diffusion in series results in a P_{crit} curve that is the sum of the two curves corresponding to the single steps, and thus exhibits a minimum at an intermediate temperature (Fig. 3C).

This additive nature of the P_{crit} curve resulting from a linear supply chain can also be derived analytically from the system of model ODEs for more than two supply steps (details in SI). Conceptually, this property can be thought of as analogous to an electrical circuit in which a fixed voltage is applied to a series of resistors. Just like the total voltage can be obtained as the sum of the individual voltage drops across each resistor, the total P_{crit} curve of a multi-step supply chain can be obtained as the sum of the pO_2 drops that drive each individual supply process.

Therefore, a bowl-shaped P_{crit} curve can emerge if the supply chain includes processes that are both more and less sensitive to temperature changes than metabolism. In Fig. 3C, the P_{crit} curve

rises under warm conditions because a large pO_2 gradient is required to drive sufficient diffusion at high temperatures. This is due to the fact that diffusion accelerates slower than metabolism with warming. On the other hand, the curve also remains flat or even reverses under cold conditions because a large pO_2 gradient is required to drive sufficient ventilation at low temperatures, since this process has a higher temperature sensitivity than metabolism.

Because the critical pO_2 differences required to drive the individual supply steps are not the same, the total P_{crit} curve is not equally sensitive to changes in the biologically controlled rate coefficients at all temperatures. In the example above, the change in P_{crit} at high temperatures due to a change in ventilation rate might be small or even negligible while its response to a change in diffusivity might be substantial, even for the same relative increase in the biologically controlled parameter. More generally, a change in the coefficient of any supply process that accelerates faster with warming than metabolism will have the largest impact on P_{crit} under cold conditions, as in the case of ventilation. On the other hand, such an increase has the largest impact on P_{crit} under warm conditions for a supply process that accelerates slower than metabolism, such as diffusion.

This relationship is particularly important for processes under immediate biological control like ventilation and circulation and has implications for understanding their temperature sensitivity. Incurring the energetic costs of accelerating heart rate or ventilation across the entire temperature range may not be beneficial if P_{crit} is instead much more sensitive to changes in diffusion at high temperatures. We illustrate this in a model variant with a ventilation rate that has a high temperature sensitivity at low temperatures but reaches an upper limit under warm conditions, as for example observed in (32, 33, 34). The resulting change in P_{crit} at high temperatures compared to a simple exponential ventilation rate is minimal (Fig. S3). In this scenario, increasing the ventilation rate throughout the warm side of the temperature range barely impacts hypoxia tolerance, because P_{crit} is largely determined by diffusion.

Evidence from Physiology

To determine whether the physiological conditions for a thermal optimum in hypoxia tolerance are common among marine biota, we compiled experimental data on the temperature dependence of ventilation and circulation rates of aquatic water breathers (Materials and Methods).

The compilation covers 58 data sets from 35 species, including 21 chordates, 9 arthropods, 3 annelids and 2 mollusks. Estimates of the sensitivity parameters (E_V, E_C) obtained by fitting Arrhenius functions to the data show an increase in ventilatory and circulatory activity with temperature in almost all species, with sensitivities ranging from -0.14 eV to 0.9 eV and a mean of 0.39 eV (± 0.22 eV SD). Since these estimates include frequencies and stroke volumes in addition to volumetric flow rates, they represent a lower bound on the actual sensitivity of ventilation and circulation as considered in the dynamic model. A higher sensitivity (0.49 eV ± 0.21 eV SD) is obtained if only volumetric rates (n =12) are considered (Fig. 4).

These results can be compared to existing estimates of the temperature sensitivity of metabolism (E_M) with a mean of 0.71 eV [± 0.46 eV SD] from a diverse set of 186 species (14). If the traits of O_2 supply and demand were independent, the estimated frequency distributions in Fig. 4 would suggest that the conditions for thermal optima ($E_V, E_C > E_M$) are met in about 23 % of species after accounting for the effect of decreasing solubility with temperature (SI). However, supply sensitivities exceed that of demand in 7 of 17 species for which both estimates are available (Dataset S1). Thus, about 40 % of species with adequate data meet this condition for having a thermal optimum in hypoxia tolerance.

The thermal variation of ventilation and circulation rates also differs across the inhabited temperature range for many species. We estimated the temperature sensitivity of volumetric flow rates in both warm and cold temperature ranges, for all species with sufficient data (n = 10). On the cold side the mean E_V and E_C are 0.69 eV, significantly exceeding the cold side with a mean of 0.07 eV (p = 0.009). The difference remains significant if stroke volumes and frequencies are also considered (n = 40 from 25 species, Fig. S5, details in SI). Thus, the acceleration of ventilation and circulation rates slows down in the warmer half of experimental temperatures on average. This

behavior is consistent with these biophysical processes conferring little additional hypoxia tolerance at high temperatures for the associated energetic cost, with P_{crit} being most sensitive to diffusion as illustrated in the model variant for ventilation (Fig. S3). Taken together, both the high temperature sensitivity of biophysical rates (circulation and ventilation) in colder waters, and the reduction of these sensitivities in warmer waters, suggest that the condition for thermal optima are commonly found among the traits of marine species.

A Metabolic Index with Thermal Optima

We generalized the Metabolic Index (MI) introduced by Deutsch et al. (9) to account for the occurrence of complex shaped P_{crit} curves. The MI is defined as the ratio of O_2 supply to resting demand of an aquatic water-breather in its environment, and it has been applied to understand how species biogeography is shaped by climate (9, 18, 35, 36, 37). However, the original formulation is limited to exponential P_{crit} curves. Our generalized version is able to reproduce the full range of behaviors exhibited by the dynamic model, but requires a relatively small number of additional parameters, and can be calibrated from experimental data through a single equation.

While it is possible to derive the ratio of supply to demand from the model ODEs analytically (SI), the MI can also be the developed from the analogy of an electrical circuit in which a fixed voltage is applied to a series of resistors.

When considering a single supply step i, the rate of O_2 supply according to Eqn. (1) is the product of the pO_2 difference ΔpO_2 between the compartments, equivalent to a 'voltage' driving a current, and the biologically determined rate coefficient $\hat{\alpha}_i$ of the process, equivalent to a temperature-dependent 'conductance' with respect to the flow of O_2.

For the habitat to be viable, this supply rate must be equal to metabolic consumption, such that P_{crit} can be interpreted as the minimum 'voltage' required to achieve an O_2 supply matching demand given the fixed 'conductance' of the biological supply process.

In a supply chain with multiple steps in series, each step is associated with such a required voltage drop - a pO_2 difference - determined by its single step conductance. Thus, the P_{crit} of the composite

chain can be obtained as the sum of the minimum pO_2 differences of the single supply steps, as illustrated in Fig. 3C.

The temperature-dependent 'conductance' (or rate coefficient) $\hat{\alpha}_i$ of a single supply step can be expressed as $\alpha_i R(E_{S_i})$, where α_i denotes the value of the coefficient at reference temperature, which is scaled by an exponential (Arrhenius) function R with temperature sensitivity E_{S_i} [eV]. More generally, in a chain with n supply steps in series, the total conductance of the chain is the reciprocal of the sum of single step resistances. When divided by metabolic demand $\alpha_M R(T, E_m)$, the resulting expression for the generalized supply-to-demand ratio is

$$\Phi = pO_2 B^{\epsilon} \left[\frac{\alpha_M}{\alpha_i} R(E_i) \right]^{-1}, \tag{2}$$

where the α_i represent the supply rate coefficients at reference temperature and $E_i = E_M - E_{S_i}$ [eV] denote the differences between the sensitivities of metabolic demand and the supply processes. The dependence of supply and demand on body mass B is reflected in the allometric exponent ϵ as in the original index (9).

The condition for the existence of a bowl-shaped P_{crit} curve, i.e. supply steps having temperature sensitivities both less than and greater than that of metabolic demand, thus reads $E_{S_i} < E_M < E_{S_j}$ for any two supply steps i and j. Eqn. (2) can include any number of supply processes. However, we find that P_{crit} curves generated by the full model ($n = 3$) can still be appropriately represented by curves assuming only 2 steps. Adding more exponential curves does not change the qualitative range of possible P_{crit} curves beyond those of concave-up bowl shapes (Fig. S4A and C). The generalized Metabolic Index in Eqn. (2) can also reproduce P_{crit} curves that include the Hx/HxO system (Fig. S4B, D and E), because the effects of the chemical blood component on the P_{crit} curve are qualitatively the same as those of the biophysical parameters (Fig. 2C and D). In such cases, however, the parameters can no longer be associated with single steps in the supply chain, but instead capture the combined properties of the processes that limit the O_2 supply towards the cold and warm ends of the temperature range, respectively.

Connecting Physiology to Biogeography

The MI framework establishes a direct link between physiological traits and biogeographical distributions, as the range boundaries of a diverse set of species align more strongly with a specific value of the index than with either temperature or pO_2 alone (14). The generalized MI has the potential to further improve this description of species habitats, especially at the cold edges of a species distribution.

To examine whether the thermal optima in physiological hypoxia tolerance are reflected in a species' biogeography, we investigate state-space habitats of biogeographic occurrence data from the Ocean Biodiversity Information System (38, Materials and Methods). For the species presented in Fig. 1, the environmental habitat conditions are poorly represented in large-scale datasets (Fig. S6). However, for two additional species with physiological traits suggesting a thermal optimum, the starry flounder *Platichthys stellatus* and the shrimp *Oplophorus spinosus*, adequate occurrence and environmental data are available. In *Platichthys stellatus*, estimates from published experimental results yield a temperature sensitivity $E_M = 0.68$ eV for metabolism and $E_{Vent} = 0.9$ eV (39) for the ventilation rate, indicating a bowl-shaped O_2 limitation. For *Oplophorus spinosus*, critical O_2 pressures have been measured and display a minimum at intermediate temperatures (40), such that Eqn. (2) can be fit directly.

In both species, the environmental conditions in occupied habitats reveal a clear minimum in inhabited pO_2 at intermediate temperatures, consistent with the physiological predictions (Fig. 5). In contrast, the minimum inhabited temperatures of each species are inconsistent with a model based on a singular lower threshold value of temperature. Instead, minimum temperatures decrease to lower values as oxygen levels increase. Similar patterns are also observed in 3 more species for which laboratory experiments indicate thermal optima and for which sufficient occurrence data are available (SI, Fig. S7). Recent state-space mapping by Duncan et al. also yielded a bowl-shaped pattern in accordance with respirometry results, and the authors used a piece-wise calibration of the MI to capture this effect (18).

In all these cases, the generalized MI reveals how the reversal in hypoxia tolerance at low temper-

atures results from physiological traits, and how this bidirectionality is reflected in biogeographic ranges. In particular, it suggests O_2 limitation is the mechanism that restricts habitat towards the cold edges of species distributions.

Discussion

The dynamic model of temperature-dependent hypoxia reveals that a linear chain of biophysical O_2 supply steps can give rise to thermal optima in hypoxia tolerance as observed in new respirometry data. This occurs when the supply chain includes at least two processes such that one accelerates with temperature more slowly than metabolic demand, and another accelerates more rapidly. In this case, the process with a lower temperature sensitivity drives an increase in P_{crit} under warm conditions, while the more sensitive process leads to a reversal with higher P_{crit} in cold waters. A generalized Metabolic Index adequately captures these complex patterns in a single metric based on mechanistic principles.

Our analysis of available physiological evidence suggests that such bidirectional effects of temperature on hypoxia tolerance may not be uncommon in aquatic animals across taxonomic groups. In addition to the presentation of new bowl-shaped P_{crit} curves, our estimates of the temperature sensitivity of ventilation and circulation rates in aquatic ectotherms fall above diffusive gas exchange and below metabolism on average, but imply the existence of thermal optima in a significant fraction of species. However, these results rely on limited physiological data. In particular, there are only a few teleost and crustacean species for which all required physiological estimates are available. Thus, sampling the involved traits across a broader range of the taxonomic, morphological and ecological diversity is a key step towards further advancing and testing this framework and its implications.

In contrast to the sparsity of detailed physiological measurements, global occurrence data is available for a much larger number and diversity of marine species (e.g OBIS). The generalized MI offers further improvements in the analysis of these data compared to its original formulation, especially along the cold edges of species habitats by including a meaningful representation of O_2 limitation

at low temperatures. In case studies presented here, thermal optima in physiological hypoxia tolerance are also reflected in species' biogeographic state space. Leveraging this approach in a future database-wide analysis of occurrence data will contribute to a fuller picture of how temperature and oxygen shape the biogeography and ecology of marine species.

Oxygen limitation of aerobic metabolism at low temperature has broad implications for marine ecosystems and their response to climate change. Marine species richness is generally observed to decline towards the poles, and is often cited as being driven by gradients in ocean temperature, with cooler waters taken to inhibit diversity (41). Our results indicate that long-term aerobic energy constraints on viable habitat in cold water might potentially represent the ultimate physiological cause of this poleward diversity loss. At the same time, warming at species' poleward range limits would relieve such aerobic constraints, allowing species to disperse towards, and establish in, higher latitudes. This mechanism could thus potentially explain widespread poleward migrations of marine species seen in response to recent anthropogenic warming (6, 42). On longer timescales, O_2 limitation at species' cold edge habitat limits provides a novel mechanism for driving habitat loss during periods of global cooling, and may potentially underlie previous extinctions during such phases (43, 44).

Materials and Methods

Laboratory Measurements. Critical O_2 levels were measured following standard closed system respirometry protocols (17, 45) for individuals of *T. tubifex* (n = 132), *N. vectensis* (n = 107) and *L. pictus* (n = 40). For the social squid *D. opalescens*, we measured critical O_2 levels for 14 groups of 15 to 30 (median 20) animals following published closed system respirometry protocols for this species (46). P_{crit} was determined by breakpoint analysis of the O_2 draw down curve (47). Full protocols are provided in the SI.

Dynamic Model. The pools and fluxes of O_2 in a generic water-breather are described by a nonlinear system of 8 ordinary differential equations. For each set of model parameters, simulations

are performed across the temperature range from 0 °C to 30 °C until P_{crit} can be determined by breakpoint analysis from the rate of O_2 draw down. All simulations were carried out in the Python language using the solve_ivp function in Scipy (48) for numerical integration. The full model description is provided in the SI.

Ventilation and Circulation Data. We compiled data on ventilation rates (n = 8), ventilation frequency (n = 18), ventilation stroke volumes (n = 6), circulation rates (n = 4), heart rates (n = 20) and heart stroke volumes (n = 2) of aquatic water-breathers measured at two or more temperatures at atmospheric O_2 levels. Estimates of the sensitivity parameters E_V, E_C were obtained through least square fits of Arrhenius functions to the experimental data using the curve_fit function and density estimates were obtained using the gaussian_kde function in Scipy. A detailed description of the compiled data is provided in the SI and all estimates are availabe in Dataset S1.

State-space Habitats. State-space habitats were obtained by pairing species location data downloaded from the Ocean Biodiversity Information System (38) in September 2019 with monthly temperature and O_2 conditions from the World Ocean Atlas (49, 50) according to the procedure described in (14). All available state-space habitats are shown in Fig. S6 and Fig. S7. Additional information is provided in the SI.

References

[1] Domingues CM, et al. (2008) Improved estimates of upper-ocean warming and multi-decadal sea-level rise. *Nature* 453(7198):1090–1093.

[2] Cheng L, Abraham J, Hausfather Z, Trenberth KE (2019) How fast are the oceans warming? *Science* 363(6423):128–129.

[3] Breitburg D, et al. (2018) Declining oxygen in the global ocean and coastal waters. *Science* 359(6371):eaam7240.

[4] Bopp L, et al. (2013) Multiple stressors of ocean ecosystems in the 21st century: projections with CMIP5 models. *Biogeosciences* 10(10):6225–6245.

[5] Gillooly JF, Brown JH, West GB, Savage VM, Charnov EL (2001) Effects of size and temperature on metabolic rate. *Science* 293(5538):2248–2251.

[6] Sunday JM (2012) Thermal tolerance and the global redistribution of animals. *Nature Climate Change* p. 6.

[7] Diaz RJ, Rosenberg R (2008) Spreading Dead Zones and Consequences for Marine Ecosystems. *Science* 321(5891):926–929.

[8] Seibel BA (2011) Critical oxygen levels and metabolic suppression in oceanic oxygen minimum zones. *J Exp Biol* 214(2):326–336.

[9] Deutsch C, Ferrel A, Seibel B, Portner HO, Huey RB (2015) Climate change tightens a metabolic constraint on marine habitats. *Science* 348(6239):1132–1135.

[10] Fry FEJ, Hart JS (1948) The relation of temperature to oxygen consumption in the goldfish. *The Biological Bulletin* 94(1):66–77.

[11] Rogers NJ, Urbina MA, Reardon EE, McKenzie DJ, Wilson RW (2016) A new analysis of hypoxia tolerance in fishes using a database of critical oxygen level (P_{crit}). *Conserv Physiol* 4(1):cow012.

[12] Wood CM (2018) The fallacy of the Pcrit – are there more useful alternatives? *J Exp Biol* p. 9.

[13] Regan MD, et al. (2019) Don't throw the fish out with the respirometry water. *J Exp Biol* 222(6):jeb200253.

[14] Deutsch C, Penn JL, Seibel B (2020) Metabolic trait diversity shapes marine biogeography. *Nature* 585(7826):557–562.

[15] Fisher TR (1976) Oxygen uptake of the solitary tunicate *Styela plicata*. *The Biological Bulletin* 151(2):297–305.

[16] Wishner KF, et al. (2018) Ocean deoxygenation and zooplankton: Very small oxygen differences matter. *Sci. Adv.* 4(12):eaau5180.

[17] Boag TH, Stockey RG, Elder LE, Hull PM, Sperling EA (2018) Oxygen, temperature and the deep-marine stenothermal cradle of Ediacaran evolution. *Proc. R. Soc. B* 285(1893):20181724.

[18] Duncan MI, James NC, Potts WM, Bates AE (2020) Different drivers, common mechanism; the distribution of a reef fish is restricted by local-scale oxygen and temperature constraints on aerobic metabolism. *Conservation Physiology* 8(1):coaa090.

[19] Dell AI, Pawar S, Savage VM (2011) Systematic variation in the temperature dependence of physiological and ecological traits. *Proceedings of the National Academy of Sciences* 108(26):10591–10596.

[20] Verberk WCEP, Bilton DT, Calosi P, Spicer JI (2011) Oxygen supply in aquatic ectotherms: Partial pressure and solubility together explain biodiversity and size patterns. *Ecology* 92(8):1565–1572.

[21] Portner HO (2010) Oxygen- and capacity-limitation of thermal tolerance: a matrix for integrating climate-related stressor effects in marine ecosystems. *J Exp Biol* 213(6):881–893.

[22] Pörtner HO, Bock C, Mark FC (2017) Oxygen- and capacity-limited thermal tolerance: bridging ecology and physiology. *J Exp Biol* 220(15):2685–2696.

[23] Zeidberg L (2013) *Advances in Squid Biology, Ecology and Fisheries. Part I – Myopsid Squids*. pp. 159–204.

[24] Wells R (2009) Chapter 6 Blood-Gas Transport and Hemoglobin Function: Adaptations for Functional and Environmental Hypoxia. *Fish Physiology* 27:255–299.

[25] Kielland yN, Bech C, Einum S (2019) Warm and out of breath: Thermal phenotypic plasticity in oxygen supply. *Funct Ecol* 33(11):2142–2149.

[26] Childress JJ, Seibel BA (1998) Life at stable low oxygen levels: adaptations of animals to oceanic oxygen minimum layers. *J Exp Biol* 201(8):1223–1232.

[27] Nilsson GE (2007) Gill remodeling in fish - a new fashion or an ancient secret? *J Exp Biol* 210(14):2403–2409.

[28] Wootton TP, Sepulveda CA, Wegner NC (2015) Gill morphometrics of the thresher sharks (Genus *Alopias*): Correlation of gill dimensions with aerobic demand and environmental oxygen: Thresher Shark Gill Dimensions. *Journal of Morphology* 276(5):589–600.

[29] Filho DW, et al. (1992) Comparative hematology in marine fish. *Comparative Biochemistry and Physiology Part A: Physiology* 102(2):311–321.

[30] Mislan KaS, Dunne JP, Sarmiento JL (2016) The fundamental niche of blood oxygen binding in the pelagic ocean. *Oikos* 125(7):938–949.

[31] Reemeyer JE, Rees BB (2019) Standardizing the determination and interpretation of P_{crit} in fishes. *J Exp Biol* 222(18):jeb210633.

[32] Kristensen E (1983) Ventilation and oxygen uptake by three species of Nereis (Annelida: Polychaeta). II. Effects of temperature and salinity changes. *Marine Ecology Progress Series* 12:299–306.

[33] Melzner F, Bock C, Pörtner HO (2006) Temperature-dependent oxygen extraction from the ventilatory current and the costs of ventilation in the cephalopod Sepia officinalis. *J Comp Physiol B* 176(7):607–621.

[34] Gehrke P (1988) Response surface analysis of teleost cardio-respiratory responses to temperature and dissolved oxygen. *Comparative Biochemistry and Physiology – Part A: Physiology* 89(4):587–592.

[35] Penn JL, Deutsch C, Payne JL, Sperling EA (2018) Temperature-dependent hypoxia explains biogeography and severity of end-Permian marine mass extinction. *Science* 362(6419):eaat1327.

[36] Howard EM, et al. (2020) Climate-driven aerobic habitat loss in the California Current System. *Sci. Adv.* 6(20):eaay3188.

[37] Oschlies A (2021) A committed fourfold increase in ocean oxygen loss. *Nat Commun* 12(1):2307.

[38] OBIS (2019) Ocean biodiversity information system. *Intergovernmental Oceanographic Commission of UNESCO*.

[39] Watters KW, Smith LS (1973) Respiratory dynamics of the starry flounder Platichthys stellatus in response to low oxygen and high temperature. *Mar. Biol.* 19(2):133–148.

[40] Cowles DL, Childress JJ, Wells ME (1991) Metabolic rates of midwater crustaceans as a function of depth of occurrence off the Hawaiian Islands: Food availability as a selective factor? *Mar. Biol.* 110(1):75–83.

[41] Tittensor DP, et al. (2010) Global patterns and predictors of marine biodiversity across taxa. *Nature* 466(7310):1098–1101.

[42] Pinsky ML, Selden RL, Kitchel ZJ (2020) Climate-Driven Shifts in Marine Species Ranges: Scaling from Organisms to Communities. *Annu. Rev. Mar. Sci.* 12(1):153–179.

[43] Saupe EE, et al. (2020) Extinction intensity during Ordovician and Cenozoic glaciations explained by cooling and palaeogeography. *Nat. Geosci.* 13(1):65–70.

[44] Reddin CJ, Kocsis dT, Kiessling W (2019) Climate change and the latitudinal selectivity of ancient marine extinctions. *Paleobiology* 45(1):70–84.

[45] Elder LE, Seibel BA (2015) Ecophysiological implications of vertical migration into oxygen minimum zones for the hyperiid amphipod *Phronima sedentaria*. *J. Plankton Res.* 37(5):897–911.

[46] Burford BP, Carey N, Gilly WF, Goldbogen JA (2019) Grouping reduces the metabolic demand of a social squid. *Mar Ecol Prog Ser* 612:141–150.

[47] Muggeo VMR (2008) segmented: an R Package to Fit Regression Models with Broken-Line Relationships. *R News* 8(1):20–25.

[48] Virtanen P, et al. (2020) SciPy 1.0: Fundamental Algorithms for Scientific Computing in Python. *Nature Methods* 17:261–272.

[49] Locarnini RA, et al. (2013) World ocean atlas 2013, volume 1: Temperature. *NOAA Atlas NESDIS* 73:40 pp.

[50] Garcia HE, et al. (2013) World ocean atlas 2013, volume 3: Dissolved oxygen, apparent oxygen utilization, and oxygen saturation. *NOAA Atlas NESDIS* 75:27 pp.

Figures and Tables

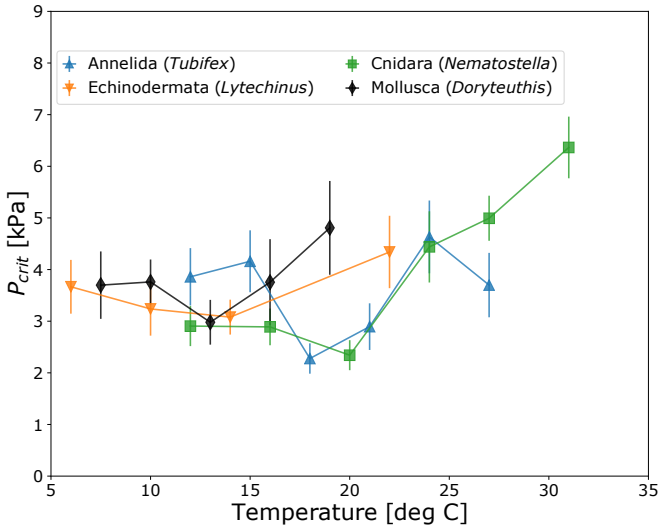

Fig. 1. Temperature-dependent critical oxygen pressures (P_{crit}, mean ± SE) of 4 marine invertebrate species from new closed-system respirometry experiments exhibit a minimum at intermediate temperatures, indicating a thermal optimum in hypoxia tolerance. The species include an oligochaete worm (*Tubifex tubifex*), a sea urchin (*Lytechinus pictus*), an anemone (*Nematostella vectensis*) and a cephalopod (*Doryteuthis opalescens*). See text for details.

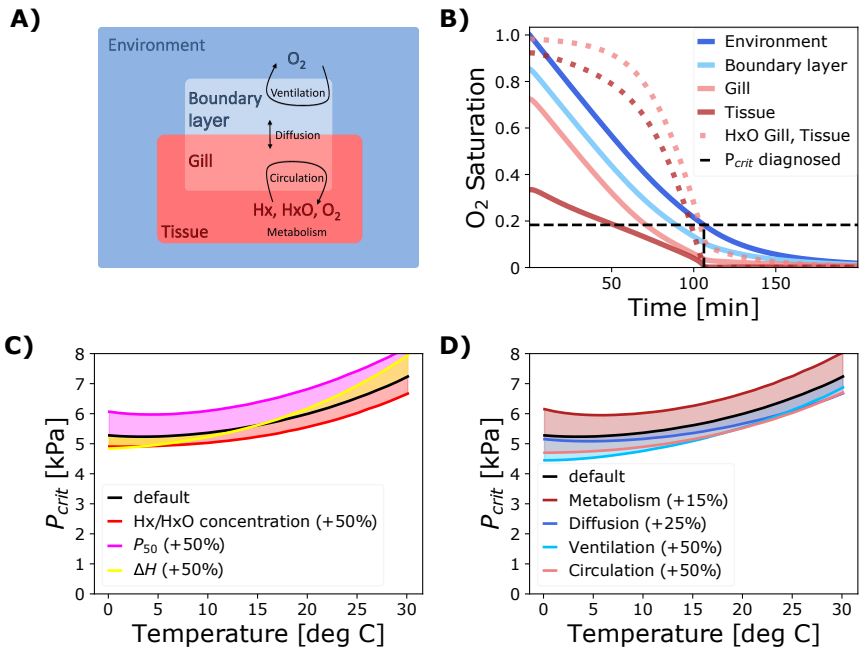

Fig. 2. Structure and output of the dynamical model used to investigate the effects of a multi-step O_2 supply chain. **A)** The model tracks the concentrations of O_2 as well as unbound and bound O_2 transporting proteins ('Hx', 'HxO') in 4 compartments representing external and internal volumes of water or body fluid, which are connected through a linear O_2 supply chain with external ventilation, diffusion and internal circulation. **B)** A model run at a single temperature resembles a closed system respirometry experiment. The saturation of O_2 (solid colored) and proportion of HxO (dashed colored) decline in all compartments until the O_2 level in the metabolizing tissue (dark red) reaches a critical limit near zero, at which point metabolic consumption slows down and P_{crit} can be determined from the rate of environmental O_2 depletion (dashed black). **C)** Effects of increasing the concentration, half-saturation pressure (P_{50}) or temperature sensitivity (ΔH) of O_2 transport protein on the P_{crit} curve. **D)** Effects of increasing the rate coefficients of biophysical supply and demand processes. A higher metabolism elevates the curve, while increasing the rate of any supply process lowers it.

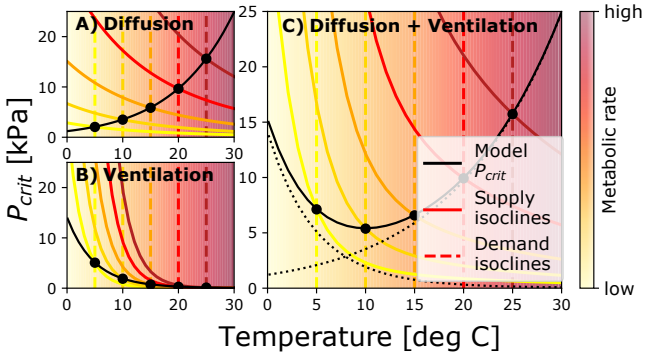

Fig. 3. Quantitative analysis of the P_{crit} curve of a model with a two-step supply chain consisting of ventilation and diffusive gas exchange. At any given temperature, the model P_{crit} can be found analytically as the intersection (dotted black) of the demand isocline (dashed colored) and the corresponding supply isocline (solid colored), aligning with the curve diagnosed from numerical simulations (solid black). **A)** In a model with only diffusive gas exchange characterized by a smaller temperature sensitivity than metabolic demand, the isocline intersections yield an increasing P_{crit} curve. **B)** Conversely, the steeper supply isoclines lead to a decreasing pattern in a single supply step model with ventilation that accelerates faster than metabolic demand. **C)** Combining the two supply steps in series results in a P_{crit} curve that is the sum of the single step curves (dotted black), giving rise to a thermal optimum at intermediate temperatures.

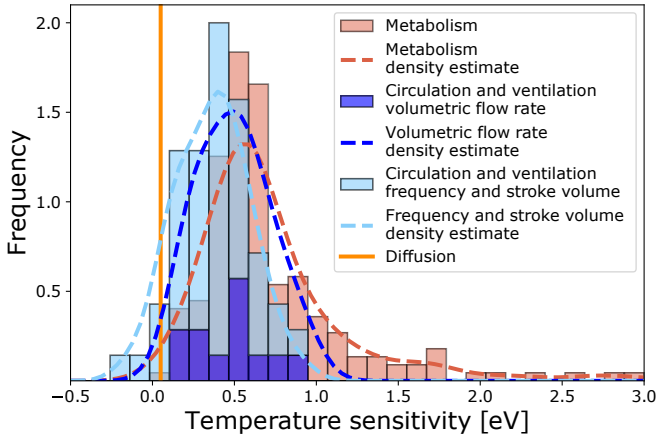

Fig. 4. The temperature sensitivities of ventilation and circulation rates estimated from published experimental data (blue, 58 estimates from 35 species) fall between the theoretical prediction for the sensitivity of diffusion (vertical orange line) and existing estimates for the sensitivity of metabolic rates (186 species, [14]) on average. Dashed lines show kernel density estimates of the trait frequency distributions.

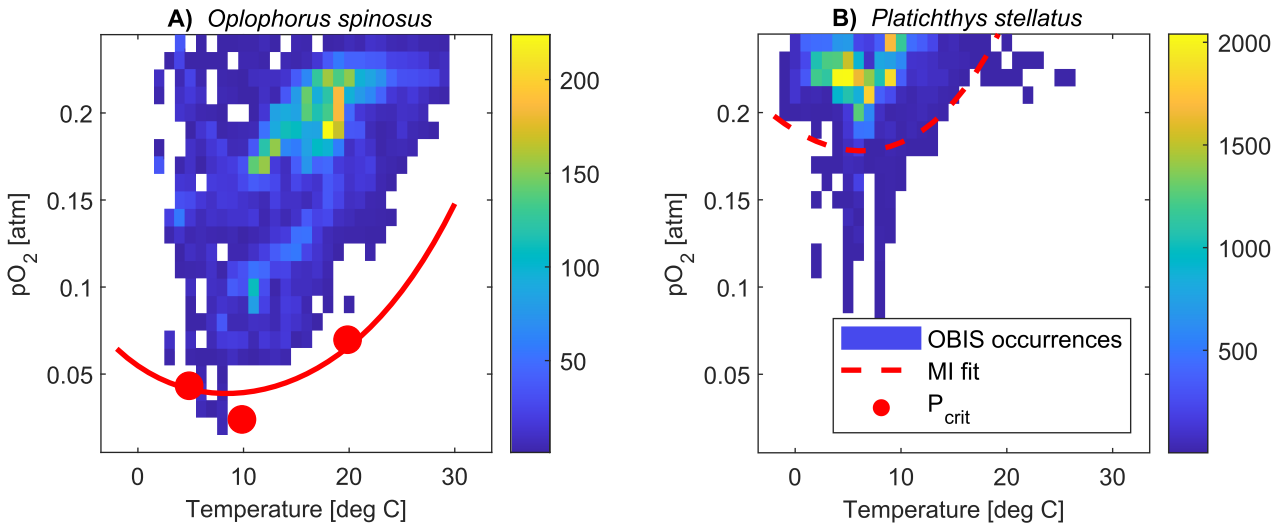

Fig. 5. Temperature and pO_2 state-space habitats using global occurrence data from the Ocean Biodiversity Information System reveal a thermal optimum at intermediate temperatures in agreement with physiological evidence. **A)** In the midwater shrimp *Oplophorus spinosus*, measured P_{crit} values (red dots) as well as the curve fit based on the Metabolic Index (solid red line) align with the lowest inhabited pO_2 across the temperature range. **B)** In the flounder *Platichthys stellatus*, the P_{crit} curve (dashed red) predicted from the MI framework and physiological rates also exhibits a thermal optimum consistent with the occurrence data.

Supplementary Information

This Supplementary Information includes:

Supplementary Text

Figures S1 to S7

Table S1

Legend for Dataset S1

SI References

Other supplementary materials for this manuscript include the following:

Dataset S1

Supplementary Information Text

A. Respiration physiology experiments

Full protocols for *Lytechinus pictus, Nematostella vectensis* and *Tubifex tubifex* by T. Boag to be included for the purpose of manuscript submission to PNAS.

Full protocols for *Doryteuthis opalescens* by B. Burford to be included for the purpose of manuscript submission to PNAS.

Full P_{crit} data for all species are shown in Fig. S1.

B. Dynamic model formulation

The time-dependent transfer of O_2 from the environment to the metabolizing tissues is simulated using a system of 8 ODEs representing the concentrations of dissolved O_2 (X) as well as the free (F) and bound (B) forms of O_2 transporting proteins in the four model compartments as shown in Fig. S2.

The full ODE system reads:

$$\text{Dissolved } O_2\ X\ : \begin{cases} V_W \frac{d}{dt} X_W &= -\hat{\alpha}_V (X_W - X_B) \\ V_B \frac{d}{dt} X_B &= \hat{\alpha}_V (x_W - X_B) - \hat{\alpha}_D \frac{(X_B - X_G)}{\kappa_H} \\ V_G \frac{d}{dt} X_G &= \hat{\alpha}_D \frac{(X_B - X_G)}{\kappa_H} - \hat{\alpha}_C (X_G - X_I) + k_b B_G - k_f X_G^n F_G \\ V_I \frac{d}{dt} X_I &= \hat{\alpha}_C (X_G - X_I) + k_b B_I - k_f X_I^n F_I - \hat{\alpha}_M \end{cases} \tag{1-4}$$

$$\text{Free transport protein } F\ : \begin{cases} V_G \frac{d}{dt} F_G &= -\hat{\alpha}_C (F_G - F_I) + k_b B_G - k_f X_G^n F_G \\ V_I \frac{d}{dt} F_I &= \hat{\alpha}_C (F_G - F_I) + k_b B_I - k_f X_I^n F_I \end{cases} \tag{5-6}$$

$$O_2 - \text{bound transport protein } B\ : \begin{cases} V_G \frac{d}{dt} B_G &= -\hat{\alpha}_C (B_G - B_I) - k_b B_G + k_f X_G^n F_G \\ V_I \frac{d}{dt} B_I &= \hat{\alpha}_C (B_G - B_I) - k_b B_I + k_f X_I^n F_I \end{cases} \tag{7-8}$$

Here X_W, X_B, X_G, X_I denote the concentrations of dissolved O_2 $[\frac{\mu mol}{l}]$ in the external water, external boundary layer, internal gill and internal tissue compartments with corresponding volumes V_W, V_B, V_G, V_I $[l]$, while F_G, F_I and B_G, B_I denote the concentrations of free and O_2-bound transport proteins $[\frac{\mu mol}{l}]$ in the gill and tissue compartments, respectively. The transport of O_2 depends on temperature $T[K]$ and is realized through ventilation $\hat{\alpha}_V(T)[\frac{l}{min}]$ between the environmental water and the boundary layer, through diffusive gas exchange $\hat{\alpha}_D(T)[\frac{\mu mol}{min\ kpa}]$ between the boundary layer and the gill volume and through circulation $\hat{\alpha}_C(T)[\frac{l}{min}]$ between the gill volume and the tissues. For diffusive gas exchange, the concentration difference between the compartments is converted to a partial pressure difference with the temperature-dependent solubility $\kappa_H(T)$ $[\frac{\mu mol}{l\ kpa}]$ of O_2 in seawater, calculated using coefficients from (1) for (2) for a salinity of 35 PSU, assuming that the relative solubility of O_2 in blood does not change with temperature for the purposes of this model (while O_2 solubility is lower in body fluid than in seawater, e.g. (3), any temperature-independent effect only changes the rate constant of diffusion). Finally, O_2 is consumed in the tissue compartment through metabolism $\hat{\alpha}_M$ $[\frac{\mu mol}{min}]$.

These supply and demand rates $\hat{\alpha}_V, \hat{\alpha}_D, \hat{\alpha}_C, \hat{\alpha}_M$ are defined as

$$\begin{aligned} \hat{\alpha}_V(T) =& \alpha_V \cdot R(T, E_V) \\ \hat{\alpha}_D(T) =& \alpha_D \cdot R(T, E_D) \\ \hat{\alpha}_C(T) =& \alpha_C \cdot R(T, E_C) \\ \hat{\alpha}_M(T) =& \alpha_M \cdot R(T, E_M) \end{aligned} \tag{9-12}$$

with constants α_x and dimensionless temperature dependent factors taking the form of Arrhenius functions

$$R(T, E_x) = \exp\left(\frac{-E_x}{k_B}(\frac{1}{T} - \frac{1}{T_{ref}})\right) \tag{13}$$

with temperature sensitivities E_x $[eV]$. Throughout the paper, we use the reference temperature $T_{ref} = 288.15$ $[^\circ K] \equiv 15$ $[^\circ C]$ and k_B denotes the Boltzmann constant. The temperature-independent α_x represent the supply and demand fluxes at the reference temperature determined by biological traits like resting metabolic rate, gill surface area, heart rate etc. These rate coefficients and temperature sensitivities are varied throughout the investigation to explore their impacts on hypoxia tolerance. For diffusion, we estimate E_D by fitting an Arrhenius function to relative diffusivity (κ) values

$$\frac{\kappa(T)}{\kappa(T_{ref})} = \frac{T}{T_{ref}} \frac{\mu(T_{ref})}{\mu(T)} \tag{14}$$

with the dynamic viscosity of seawater $\mu(T)$ calculated according to (4) for a salinity of 35 PSU. After accounting for temperature-dependent solubility κ_H, this yields a value of $E_D \approx 0.06$ eV. Typical values of the biophysical parameters and values used for the compartment volumes are provided in Table S1.

The model also contains a blood component with free (F) and bound (B) forms of transport

protein circulating between the gill and the tissue compartments according to $\hat{\alpha}_C(T)$. These bind or release O_2 with forward and backward reaction rates k_f $[\frac{l^3}{\mu mol^2\ min}]$, k_b $[\frac{l}{min}]$, respectively, with a dissociation curve following Hill's equation where the O_2 pressure producing half-saturation, denoted P_{50}, is temperature-dependent (5). The fraction Y of protein bound to O_2 is

$$Y = \frac{[B]}{[B] + [F]} = \frac{pO_2^{n_H}}{P_{50}^{n_H} + pO_2^{n_H}} \tag{15}$$

where

$$P_{50}(T) = P_{50}^{T_{ref}} \cdot \exp\left(\frac{\Delta H}{R_{Gas}}(\frac{1}{T} - \frac{1}{T_{ref}})\right) \tag{16}$$

with the half-saturation pressure at the reference temperature $P_{50}^{T_{ref}}$, the Hill coefficient n_H and the enthalpy of the binding reaction ΔH, and the gas constant R_{Gas}. The O_2 concentration K_{50} producing half saturation ('microscopic dissociation constant') can be converted from the pressure $K_{50} = \kappa_H P_{50}$. Since the ratio of the reaction rates k_f, k_b determining the equilibrium is more relevant than the absolute values of the rates for our purposes, we fix the forward rate to be much faster than diffusive gas exchange and compute k_b as $k_b = k_f K_{50}^{n_H}$ from the equilibrium constant $K_{eq} = \frac{k_b}{k_f} = K_{50}^{n_H}$).

The values used for these chemical parameters are shown in Table S1.

At each temperature, we integrate the ODE system using the *solve_ivp* solver in Python (6). We start each simulation with a concentration of dissolved O_2 typical of surface seawater of 300 $\frac{\mu mol}{l}$ in all compartments and with corresponding equilibrium concentrations of the transport protein. After an initial spin-up time of 50 min with constant $X_W(t)$ to ensure that the saturated O_2 concentration can support the model metabolic rate, $X_W(t)$ starts to evolve according to SI Eqn. (1). To determine P_{crit}, we use the breakpoint analysis (7) by applying a segmented linear regression following (8) to the rate of change of $X_W(t)$. We use the time t_{crit} at which the O_2 concentration in the tissue first drops below a critical limit near zero ($X_I(t_{crit}) \leq 0.05$ $\frac{\mu mol}{l}$) as an initial guess for the single

breakpoint and restrict the regression to the interval [50, $t_{crit} + \frac{t_{crit}}{5}$]. If X_I never drops below this threshold during the default simulation time of 1000 min, the time is doubled and the process is repeated until a P_{crit} value is obtained.

To illustrate the diminishing effects of supply processes that accelerate faster than metabolism under warm condition, we formulate a simple model variant with a modified ventilation rate with a slowed acceleration above 20 °C:

$$\hat{\alpha}_V = \begin{cases} \alpha_V R(T, E_V) & T < 288.15\ K \\ \frac{2\alpha_V}{1+\exp(-\lambda(T-T_{ref})} & T \geq 288.15\ K \end{cases} \tag{17}$$

where $\lambda = \frac{2E_V}{k_B T_{ref}^2}$ is chosen to match the value and slope of the Arrhenius ventilation at T_{ref}. The modified rate as well as the resulting change in P_{crit} is shown in Fig. S3.

C. Metabolic Index derivation

The generalized Metabolic Index (Eqn. (2) in main text) can be derived from the dynamical model without the blood proteins F, B in SI Eqn. (1) to (4). To determine P_{crit} analytically, we consider the case of a very large environmental volume $V_W \to \infty$, which is equivalent to a setting with a constant environmental O_2 level $X_W(t) = X_W$ that is not depleted over time. Intuitively, this represents the fact that respiration of a small model organism does not significantly change the ambient O_2 level in the ocean or a large tank. Under this assumption, we can find the constant concentration X_W^{crit} that results in a steady state O_2 level of zero in the tissue, $X_I^{ss} = 0$, which corresponds to the criterion for reaching P_{crit} in our model. From SI Eqn (4), we have

$$\begin{aligned} \frac{d}{dt}X_I &= \hat{\alpha}_C(X_G^{ss} - 0) - \hat{\alpha}_M = 0 \\ \Rightarrow X_G^{ss} &= \frac{\hat{\alpha}_M}{\hat{\alpha}_C}. \end{aligned}$$

Substituting this in SI Eqn 3 yields

$$\frac{d}{dt}X_G = \hat{\alpha}_D \frac{(X_B^{ss} - \frac{\hat{\alpha}_M}{\hat{\alpha}_C})}{\kappa_H} - \hat{\alpha}_M = 0$$
$$\Rightarrow X_B^{ss} = \frac{\hat{\alpha}_M \kappa_H}{\hat{\alpha}_D} + \frac{\hat{\alpha}_M}{\hat{\alpha}_C}.$$

Finally, inserting X_B^{ss} and X_G^{ss} in SI Eqn. (2) yields

$$\frac{d}{dt}X_B = \hat{\alpha}_V(X_W^{crit} - \frac{\hat{\alpha}_M \kappa_H}{\hat{\alpha}_D} - \frac{\hat{\alpha}_M}{\hat{\alpha}_C}) - \hat{\alpha}_M = 0$$
$$\Rightarrow X_W^{crit} = \frac{\hat{\alpha}_M}{\hat{\alpha}_V} + \frac{\hat{\alpha}_M \kappa_H}{\hat{\alpha}_D} + \frac{\hat{\alpha}_M}{\hat{\alpha}_C}.$$

Converting to partial pressure results in the expression for P_{crit}

$$P_{crit} = \frac{\hat{\alpha}_M}{\hat{\alpha}_V \kappa_H} + \frac{\hat{\alpha}_M}{\hat{\alpha}_D} + \frac{\hat{\alpha}_M}{\hat{\alpha}_C \kappa_H} \tag{18}$$

This corresponds to the MI

$$\Phi = pO_2 B^{\epsilon} \left(\frac{\hat{\alpha}_M}{\hat{\alpha}_V \kappa_H} + \frac{\hat{\alpha}_M}{\hat{\alpha}_D} + \frac{\hat{\alpha}_M}{\hat{\alpha}_C \kappa_H} \right)^{-1} \tag{19}$$

which matches Eqn. (2) in the main text after substituting SI Eqns. (9) to (12), including the body mass dependence B^{ϵ} of the original index. On the other hand, the same result is obtained when considering the ratio of O_2 supply to demand directly, since the total (potential) supply S_{tot} of the supply chain is

$$S_{tot} = pO_2 \cdot \hat{\alpha}_{tot}$$

with the total conductance of the linear chain

$$\hat{\alpha}_{tot} = \left(\sum_{i=1}^{n} \frac{1}{\hat{\alpha}_i} \right)^{-1} .n$$

Now the ratio $\frac{S_{tot}}{\hat{\alpha}_M}$ once again yields SI Eqn. (19).

While the full system including the transport protein concentrations F, B does not yield a simple expression for P_{crit} and Φ, simulated P_{crit} curves can be adequately fit based on Eqn. 2 in the main text with only $n = 2$ supply steps, as shown in Fig. S4 for a range of biophysical and chemical parameters. In particular, the figure illustrates the fact that the presence of O_2 transporting proteins essentially enhances the supply capacity of circulation in the model, with changes in the total concentration of protein achieving a similar effect to changes in the parameter α_C (Fig. S4 A and B) and changes in the enthalpy of the binding reaction corresponding to changes in the sensitivity E_C (Fig. S4 C, D).

D. Ventilation and circulation data

We compiled data on the thermal sensitivity of ventilation rates (n=8), ventilation frequencies (n=18), ventilation stroke volumes (n=6), circulation rates (n=4), heart rates (n=20) and heart stroke volumes (n=2) in aquatic water breathers at atmospheric O_2 levels measured at 2 or more temperatures from the literature. For each of the 58 datasets from 35 species (25 marine, 10 freshwater), the temperature dependence of the measured quantity was estimated by fitting an Arrhenius equation $k \cdot R(T, E)$ from SI Eqn. (13) to the data normalized to the lowest experimental temperature and estimating the sensitivity parameter E. Least-Square Fits were performed using the *scipy.optimize.curve_fit* function. The results are provided in Dataset S1.

The temperature sensitivities of ventilation (32 estimates) and circulation (26 estimates) were not significantly different in terms of means according to a F-test ($p = 0.1608$), which was performed after testing for equal variances (Levene-test, $p = 0.8103$) and checking normality (Shapiro-Wilk-

test, $p = 0.5071$ and $p = 0.5816$, respectively). Therefore, the ventilation and circulation estimates were combined for further analysis.

We estimated the expected frequency of the supply temperature sensitivities E_V, E_C of volumetric flow rates exceeding the sensitivity of metabolism E_M. To that end, we estimated the trait frequency distributions of these sensitivities through kernel density estimation using the gaussian_kde function in Scipy and sampled from the resulting densities ($n = 100000$). To account for the effect of decreasing solubility κ_H with temperature as it appears in SI Eqn. (18), the density of ventilation and circulation rates was shifted by the temperature sensitivity of solubility (≈ 0.144 eV from 2). This procedure yields an expected frequency for $E_V, E_C > E_M$ of 23 %, which corresponds to the expected fraction of species with thermal optima in hypoxia tolerance if the traits are considered independent.

On the other hand, in the 17 species for which both estimates are available, we find that $E_V, E_C > E_M$ in 7 cases (frequency ≈ 41 %) after accounting for solubility effects, indicating that the traits determining the thermal sensitivity of O_2 supply and demand are unsurprisingly not independent in real organisms. The temperature sensitivities in these 17 species are comparable to estimates obtained from all species (demand 0.58 ± 0.15 eV, supply 0.43 eV ± 0.21 eV, Fig. S5A).

To evaluate whether E_V, E_C are themselves temperature dependent, we estimated the parameter separately above and below the median temperature in the 40 datasets from 25 species with 4 or more distinct experimental temperatures. Estimates were again obtained by fitting Arrhenius functions $k \cdot R(T, E)$ to the data. For the 10 estimates of volumetric flow rates, the cold side mean of 0.69 eV far exceeds the warm side mean of 0.07 eV (paired sample t-test, $p = 0.009$). The difference remains significant when frequencies and stroke volumes are also considered (cold side mean 0.43 eV, warm side mean of 0.15 eV, paired sample t-test, $p = 0.0085$). This is illustrated in Fig. S5B. If the analysis is restricted to the 24 datasets from 16 species with temperature ranges of

at least 5 °C both above and below the median experimental temperature, the difference between the cold side mean (0.48 eV) and the warm side mean (0.22 eV) remains similar. The average experimental temperature range is 17.95 °C (10.95 °C cold side, 7.51 °C warm side).

E. State-space projections

The curves in Fig. 5 were obtained from Eqn. (2) with $n = 2$ supply steps while accounting for any physiological evidence available for the respective species.

For *Oplophorus spinosus*, Eqn. (2) was fit directly to the experimental P_{crit} data (9) while constraining the temperature sensitivities to $0 < E_1 < 0.8$ [eV] and $-0.7 < E_2 < 0$ [eV] respectively, based on the estimate $E_M \approx 0.7308$ eV estimated in (10) from the data of (9).

For *Platichthys stellatus*, no estimates of P_{crit} are available, so the curve was tuned to $E_1 = 0.65$ eV and $E_2 = -0.25$ eV based on the available estimates of $E_{Vent} \approx 0.9$ eV and $E_M \approx 0.68$ eV, as well as the theoretical value of $E_D \approx 0.06$ eV for diffusion.

In addition to the state-space habitats shown in Fig. 5, we also provide the habitats for the 4 species with experimental P_{crit} data (Fig. 1) in Fig. S6. There are only very few occurrences available in OBIS for three of the species (*L. pictus, N. vectensis, T. tubifex*), two of which are intertidal (*N. vectensis*) or inhabit freshwater and brackish habitat (*T. tubifex*). In these cases, the use of monthly mean values for temperature and O_2 conditions from the World Ocean Atlas likely does not reflect the range of environmental conditions these species experience in their natural habitats, such as strong variations in O_2 frequently experienced by intertidal animals (11), and limits the interpretation of the state-space projections. While there is a larger number of occurrences for *D. opalescens* (Fig. S6A), the gradients in temperature and O_2 these squid experience during offshore migrations and nearshore spawning activity (12) are likely also not well represented in monthly climatologies.

Finally, we provide the state-space habitats for the 8 marine species for which both estimates of the supply and demand temperature sensitivities are available (Fig. S7, Dataset S1). The curves

shown for these species (*A. succinea*, *C. sapidus*, *C. maenas*, *C. crangon*, *G. morhua*, *O. nerka*, *S. canicula* and *S. solea*) in Fig. S7 were obtained by similar tuning to the available physiological evidence as in the case of *Platichthys stellatus* (Fig. 5), using available estimates of E_V, E_C and E_M as well as $E_D \approx 0.06$ eV for diffusion.

The state-space habitats reveal bowl-shaped patterns in the two additional marine species for which physiological evidence suggests the presence of thermal optima (*C. crangon, S. solea*). Such bowl-shaped patterns are also present in the state-space habitats of some the remaining species, for which the available estimates only explain the warm edge (e.g. *G. morhua, Fig. S7E*). However, there is no species with all required sensitivity estimates for metabolic demand, ventilation rate and circulation rate to test the emergence of state-space habitats without thermal optima.

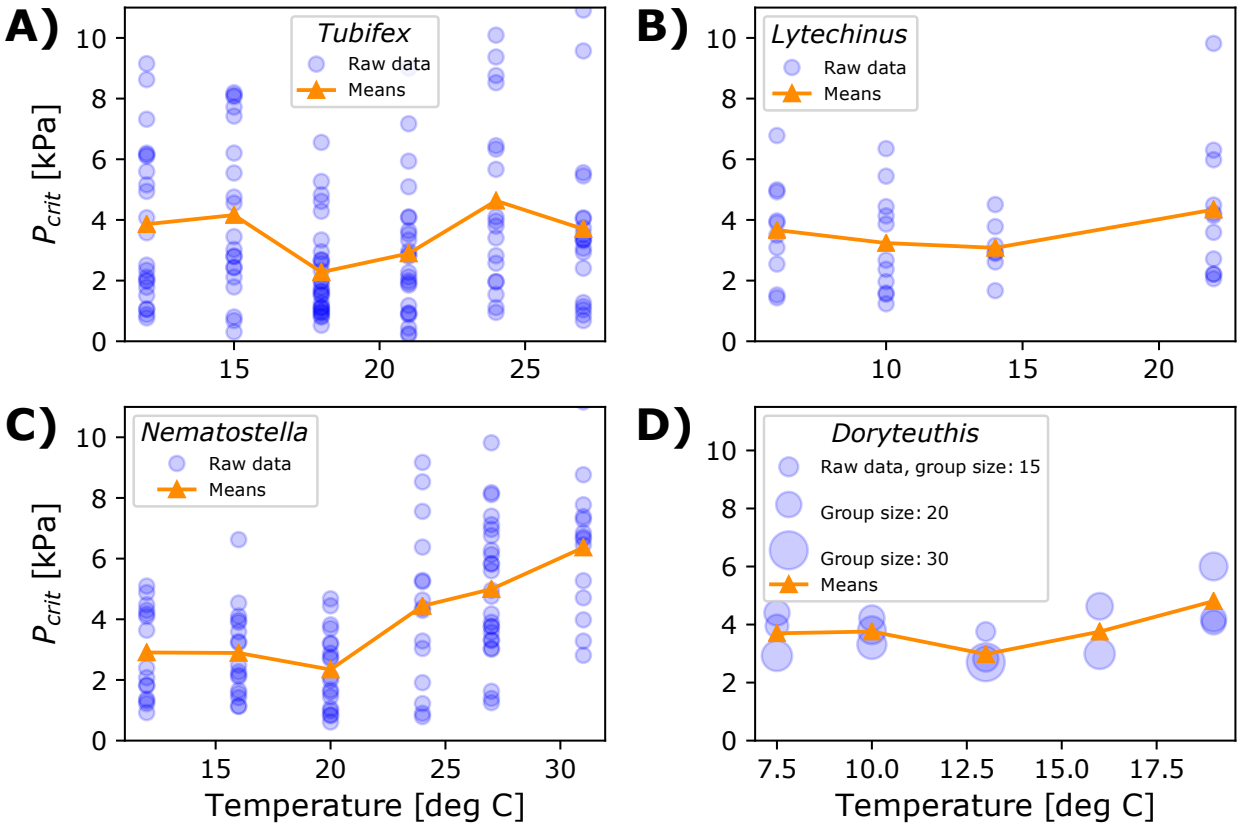

Fig. S1. Raw P_{crit} measurements (blue) and mean values as in Fig. 1 (orange) for **A)** the oligochaete worm *Tubifex tubifex*, **B)** the sea urchin *Lytechinus pictus*, **C)** the anemone *Nematostella vectensis* and **D)** the market squid *Doryteuthis opalescens*. Experimental protocols and the procedure for determining P_{crit} values are provided in SI Text A.

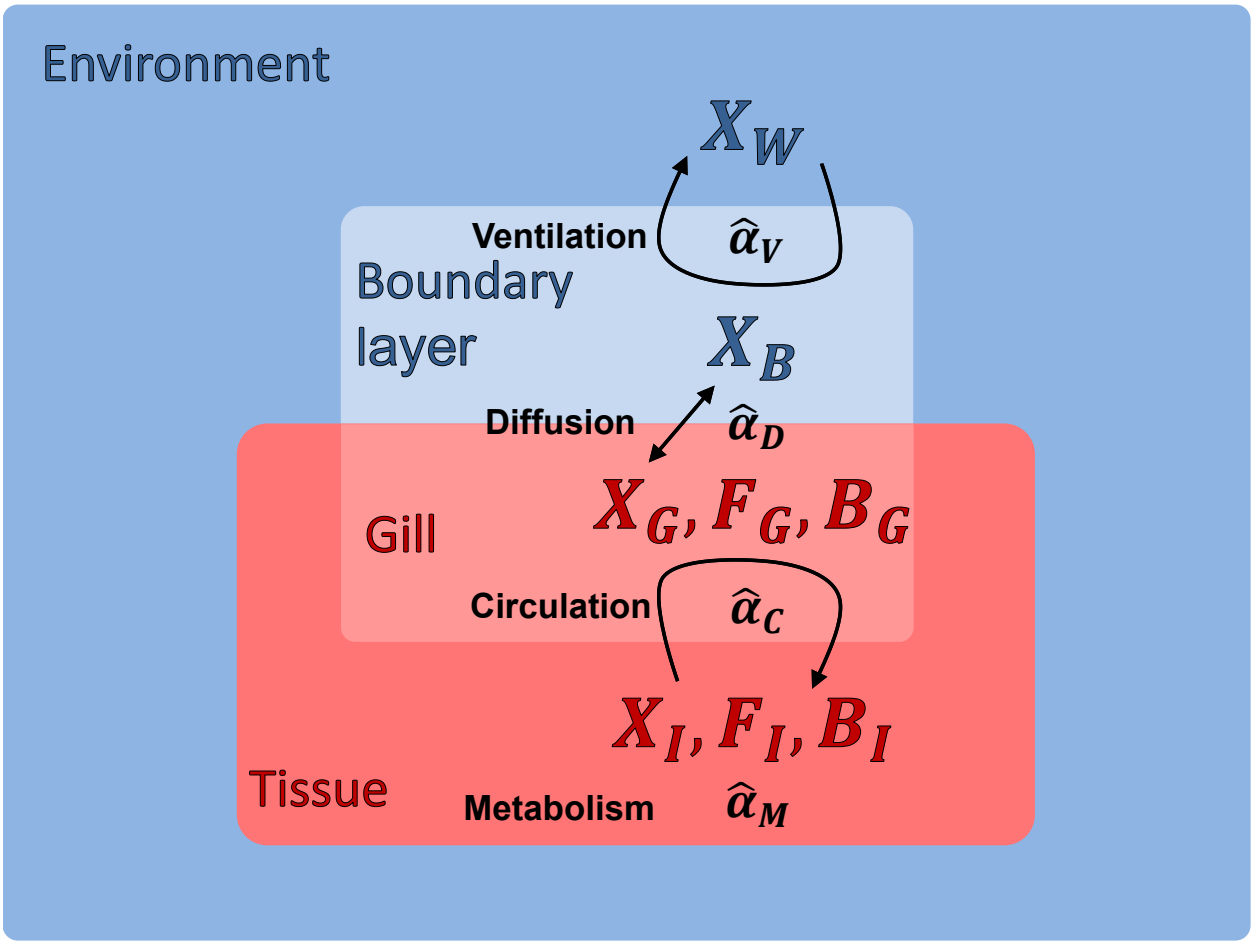

Fig. S2. Illustration of state variables for dissolved O_2 (X), free (F) and bound (B) O_2-transport protein as well as temperature-dependent O_2 supply and demand processes ($\hat{\alpha}$) used in the dynamical ODE model.

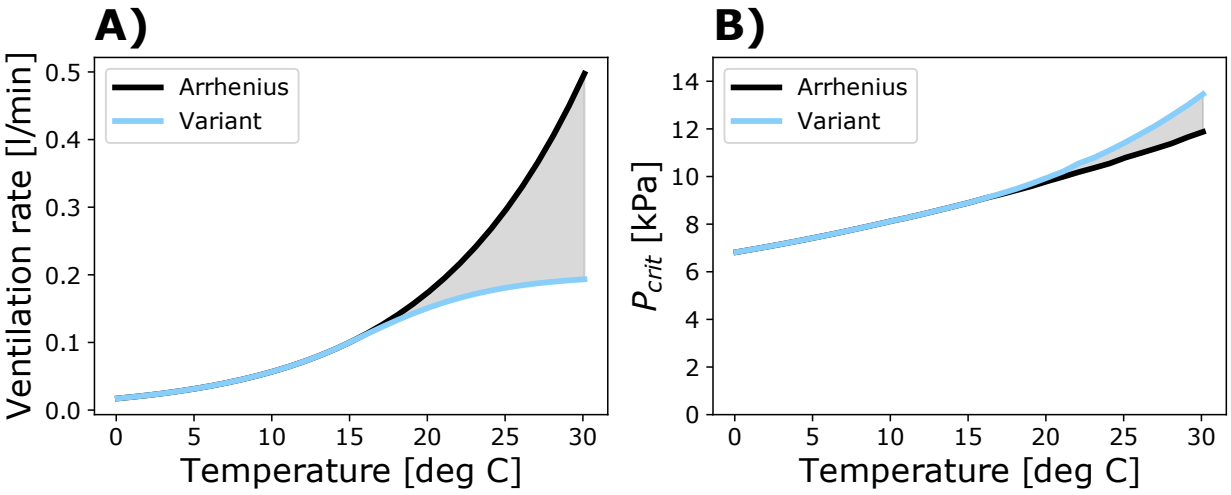

Fig. S3. Variant of the dynamical model featuring a ventilation rate with slower acceleration at high temperatures. **A)** Above 20 °C, the modified ventilation rate following SI Eqn. (17) accelerates significantly slower than the default rate governed by the exponential (Arrhenius) relationship in SI Eqn. (9). **B)** The resulting change in P_{crit} at high temperatures is minimal because ventilation is characterized by a larger temperature sensitivity than metabolism ($E_V = 0.8eV, E_M = 0.5eV$).

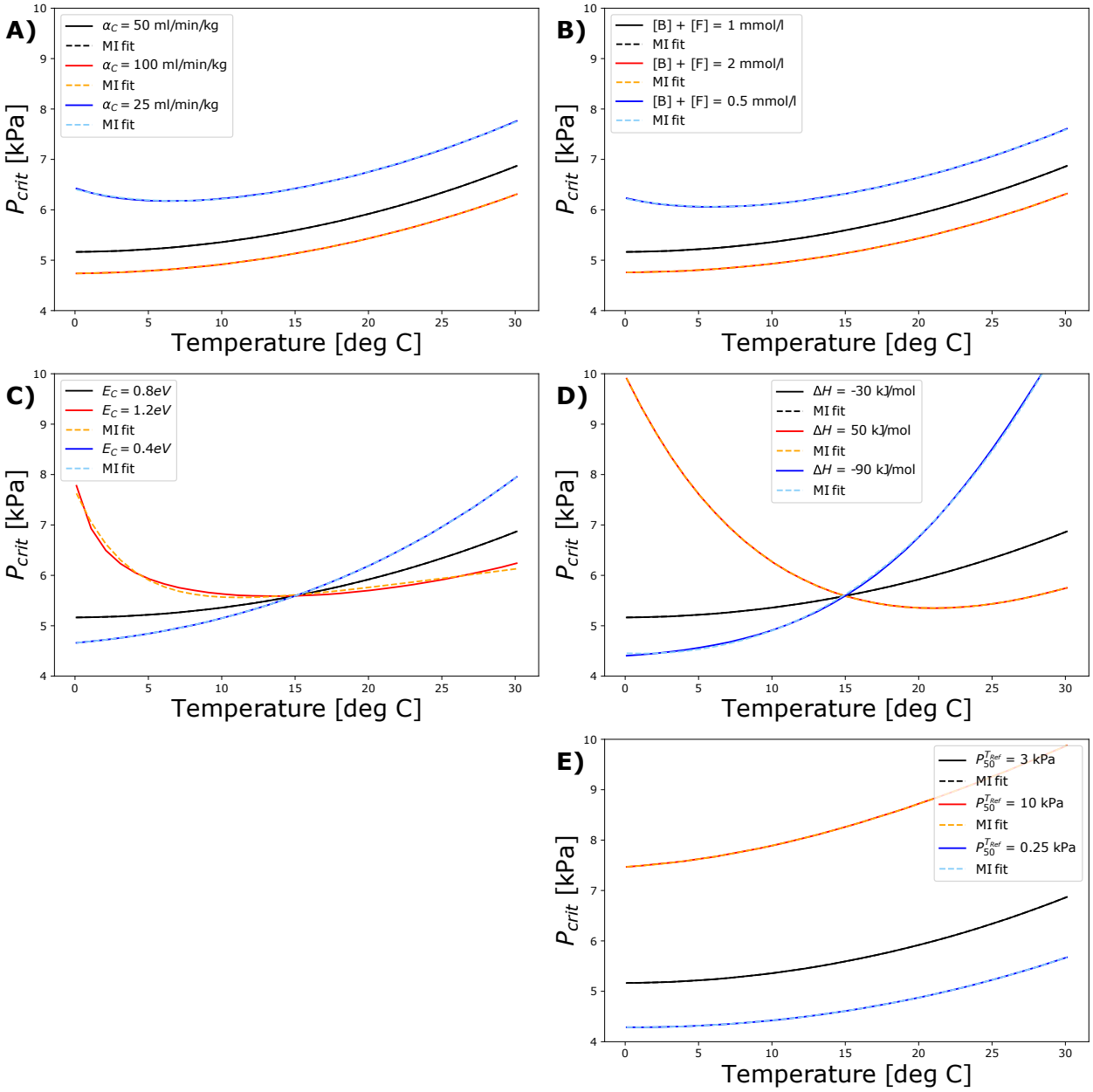

Fig. S4. Variations in the biophysical parameters governing internal circulation (left column) result in similar P_{crit} changes as variations in the chemical parameters describing the transport of O_2 by proteins (right column). Fits based on Eqn. (2) from the main text with $n = 2$ supply steps (dashed) capture the simulated P_{crit} curves. **A)** The constant α_C determines the circulation rate at the reference temperature. **B)**. Changes to the total concentration of O_2 transport protein have a similar effect as observed for α_C. **C)**. The temperature sensitivity of circulation E_C determines the slope of the Arrhenius relationship in SI Eqn. (11). **D)** The enthalpy of the binding reaction changes the effective temperature dependence of the circulation rate similar to changes in E_C. **E)** The half-saturation pressure at the reference temperature $P_{50}^{T_{Ref}}$ describes the overall affinity of the transport protein to O_2 and correspondingly affects the supply capacity.

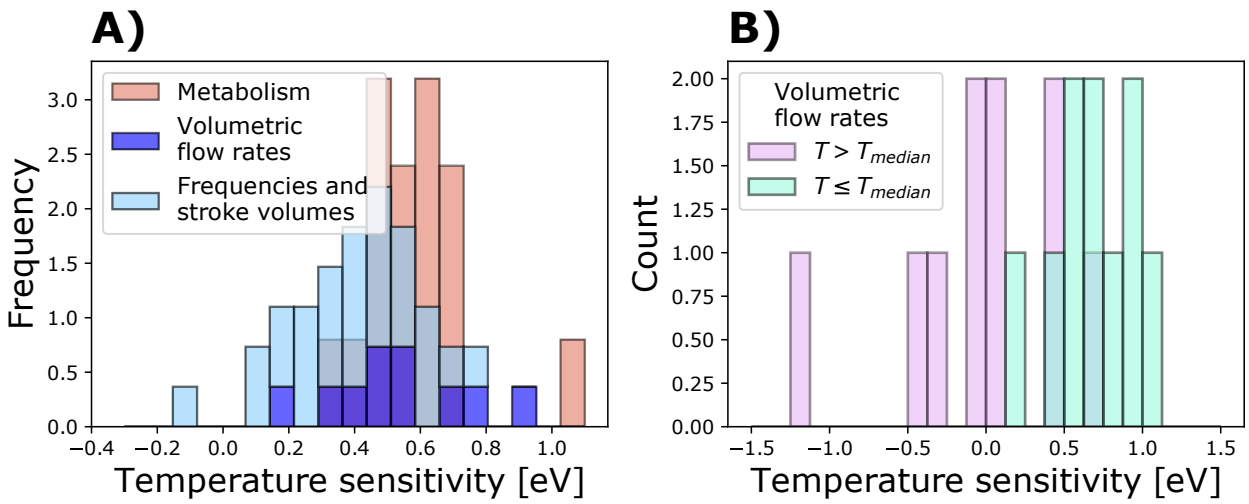

Fig. S5. Frequency distributions of additional estimated temperature sensitivities. **A)** The sensitivity estimates for ventilation and circulation as well as metabolic demand in the 17 species for which both quantities are available yield a distribution that is comparable to that obtained from all species (Fig. 4). **B)** The estimated temperature sensitivity of volumetric ventilation and circulation flow rates below the median experimental temperature far exceed that above the median experimental temperature on average, indicating that these supply processes accelerate at a faster rate under cold conditions.

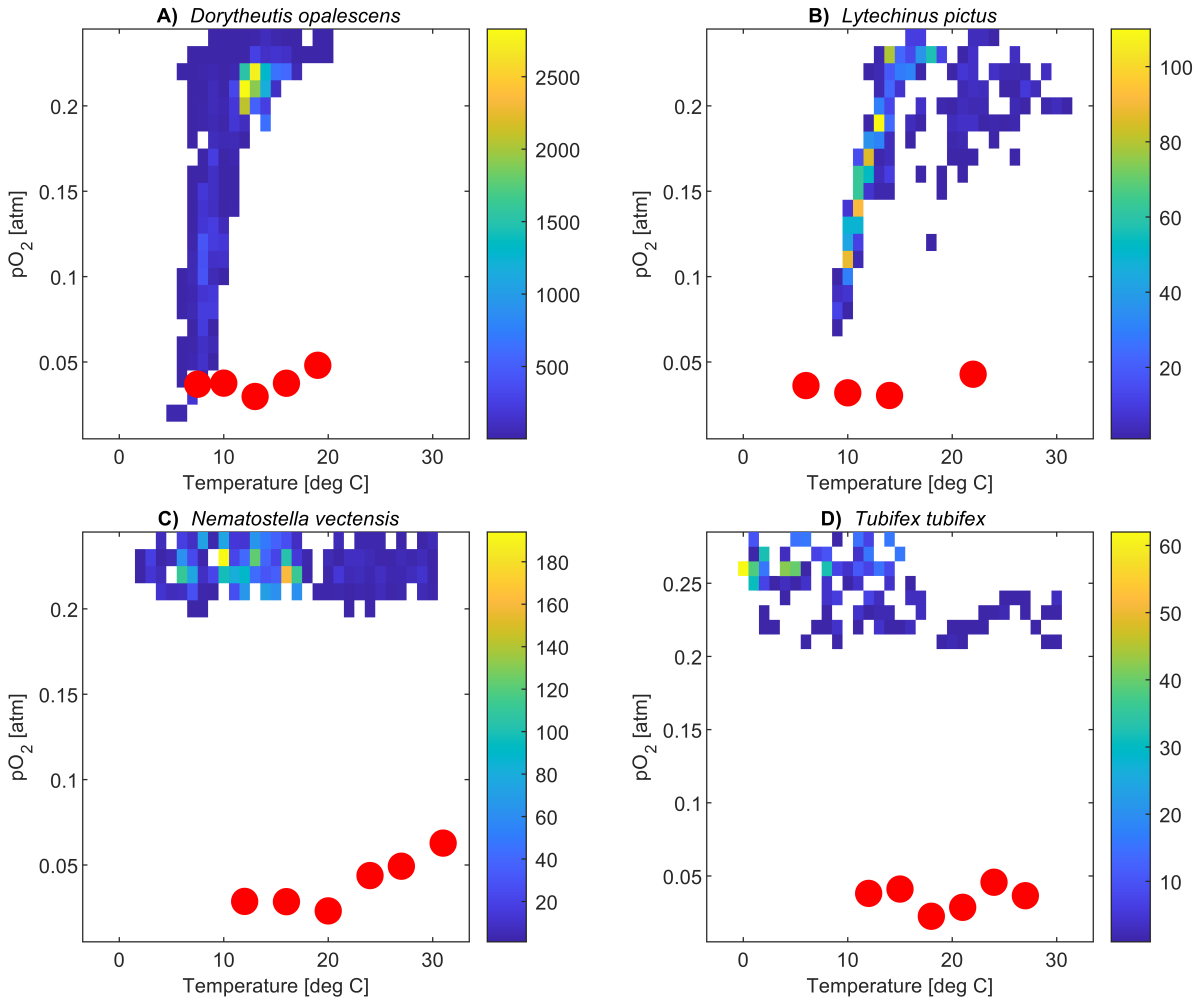

Fig. S6. State-space habitats of OBIS occurrences along with mean experimental P_{crit} values for the 4 species presented in Fig. 1, including **A)** market squid from the California Current System, **B)** an outer shelf sea urchin, **C)** an intertidal anemone and **D)** a sludge worm that mostly inhabits freshwater habitat.

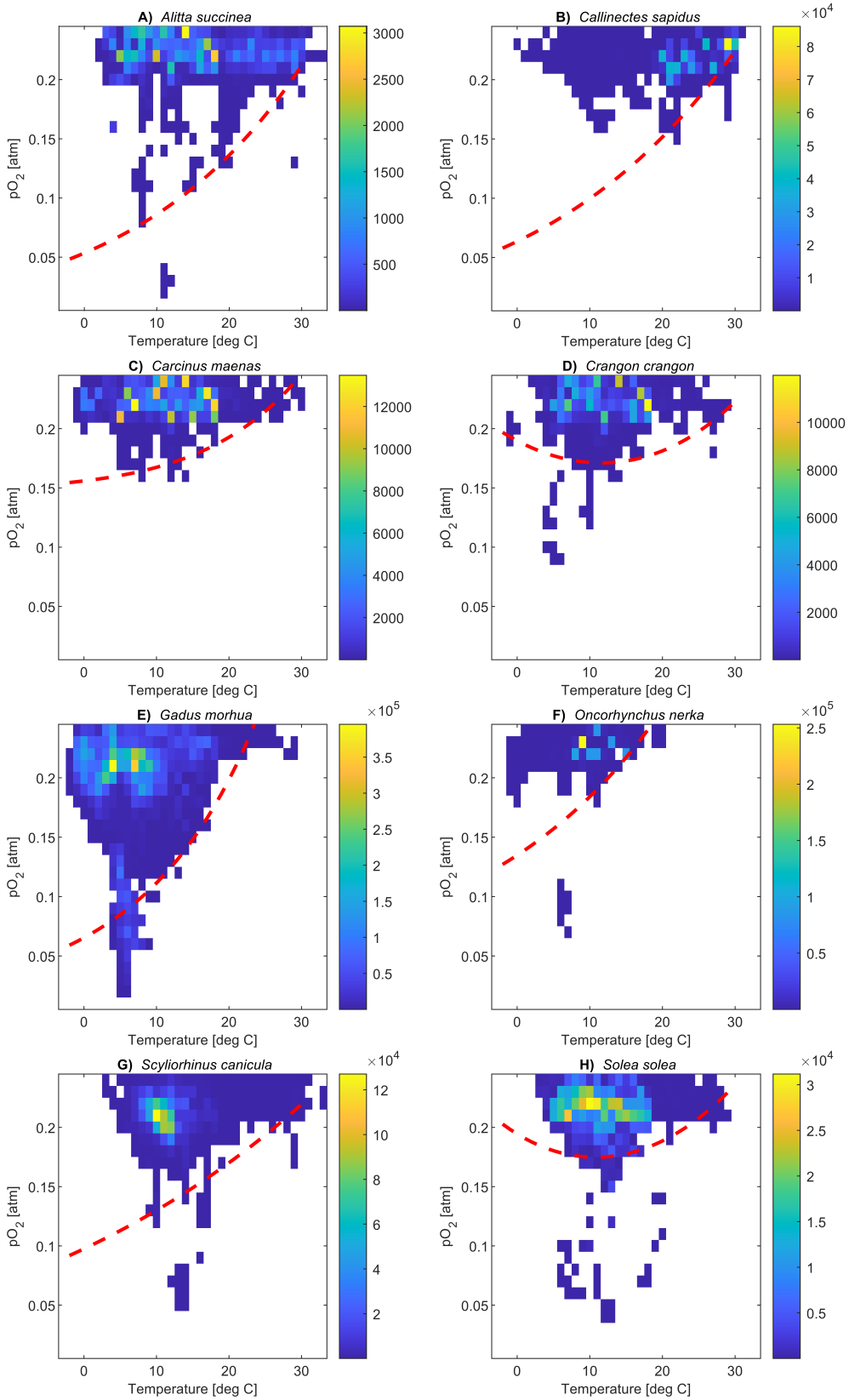

Fig. S7. State-space habitats for all species with sufficient physiological data on temperature-dependent O_2 supply and demand rates as well as occurrence data in OBIS. Red curves are based on SI Eqn. (18) tuned according to the available physiological evidence (Dataset S1).

Table S1. Descriptions and default values of state variables and parameters in the dynamical model.

	Description	Default Value	Unit
T	Temperature	273.15 – 303.15	K
k_B	Boltzmann's constant	8.6173e-5	eV/K
R_{Gas}	Gas constant	0.008314	kJ/K/mol
T_{ref}	Reference temperature	288.15	K
$\kappa_H(T)$	Solubility of O_2 in seawater	Ref. (1)	μmol/liter/kPa
μ	Dynamic viscosity of seawater	Ref. (4)	kg/min/s
X_W	O_2 Concentration in environment	300	μmol/liter
X_B	O_2 Concentration in boundary layer	300	μmol/liter
X_G	O_2 Concentration in gill	300	μmol/liter
X_I	O_2 Concentration in tissue	300	μmol/liter
F_G	Free protein concentration in gill	$(1-Y)\cdot 1$	mmol/liter
F_I	Free protein concentration in tissue	$(1-Y)\cdot 1$	mmol/liter
B_G	Bound protein concentration in gill	$Y\cdot 1$	mmol/liter
B_I	Bound protein concentration in tissue	$Y\cdot 1$	mmol/liter
V_W	Volume of environmental compartment	20	liter
V_B	Volume of boundary layer compartment	0.005	liter
V_G	Volume of gill compartment	0.005	liter
V_I	Volume of tissue compartment	0.005	liter
α_V	Ventilation rate at T_{ref}	0.002	liter/min
α_D	Diffusion rate at T_{ref}	0.029	μmol /min / kPa
α_C	Circulation rate at T_{ref}	0.00025	liter/min
α_M	(Resting) Metabolic rate at T_{ref}	0.05	μmol/liter/min
E_V	Temperature sensitivity of ventilation	0.8	eV
E_D	Temperature sensitivity of diffusion	0.21	eV
E_C	Temperature sensitivity of circulation	0.8	eV
E_M	Temperature sensitivity of metabolism	0.5	eV
$P_{50}^{T_{ref}}$	Half-saturation pressure at T_{ref}	3	kPa
Y	Fraction of bound O_2-transport protein	SI Eqn. (15)	-
n_H	Hill coefficient	2	-
ΔH	Enthalpy of O_2 binding reaction	-30	kJ/mol
K_{eq}	Equilibrium constant of O_2 binding reaction	$\frac{1}{(P_{50}\kappa_H)^{n_H}}$	μmol^2 / liter^2
k_f	Forward/O_2 binding reaction rate	10 α_D	liter^3 / μmol^2 /min
k_b	Backward/O_2 dissociation reaction rate	$k_f K_{eq}$	liter/min

SI Dataset S1 (separate file, sensitivity_estimates.csv)

Temperature sensitivity estimates from published data on ventilation and circulation in aquatic water breathers. If available, separate estimates above and below the median experimental temperature as well as estimates of the temperature sensitivity of resting metabolism are included.

SI References

[1] Garcia HE, Gordon LI (1992) Oxygen solubility in seawater: Better fitting equations. *Limnol. Oceanogr.* 37(6):1307–1312.

[2] Benson BB, Krause D (1984) The concentration and isotopic fractionation of oxygen dissolved in freshwater and seawater in equilibrium with the atmosphere1: Oxygen solubility in seawater. *Limnol. Oceanogr.* 29(3):620–632.

[3] Lallier F, Truchot J (1989) Hemolymph oxygen transport during environmental hypoxia in the shore crab, Carcinus maenas. *Respiration Physiology* 77(3):323–336.

[4] Sharqawy MH, Lienhard JH, Zubair SM (2010) Thermophysical properties of seawater: a review of existing correlations and data. *Desalination and Water Treatment* 16(1-3):354–380.

[5] Wells R (2009) Chapter 6 Blood-Gas Transport and Hemoglobin Function: Adaptations for Functional and Environmental Hypoxia. *Fish Physiology* 27:255–299.

[6] Virtanen P, et al. (2020) SciPy 1.0: Fundamental Algorithms for Scientific Computing in Python. *Nature Methods* 17:261–272.

[7] Reemeyer JE, Rees BB (2019) Standardizing the determination and interpretation of P_{crit} in fishes. *J Exp Biol* 222(18):jeb210633.

[8] Muggeo VMR (2008) segmented: an R Package to Fit Regression Models with Broken-Line Relationships. *R News* 8(1):20–25.

[9] Cowles DL, Childress JJ, Wells ME (1991) Metabolic rates of midwater crustaceans as a function of depth of occurrence off the Hawaiian Islands: Food availability as a selective factor? *Mar. Biol.* 110(1):75–83.

[10] Deutsch C, Penn JL, Seibel B (2020) Metabolic trait diversity shapes marine biogeography. *Nature* 585(7826):557–562.

[11] Mcmahon BR (1988) Physiological Responses to Oxygen Depletion in Intertidal Animals. *Am Zool* 28(1):39–53.

[12] Zeidberg L (2013) *Advances in Squid Biology, Ecology and Fisheries. Part I – Myopsid Squids*. pp. 159–204.